Int. J. Anal. Appl. (2026), 24:201

International Journal of Analysis and Applications

# Structural Graphs of Fingerprints: A Dynamical Approach

**Bouchra Tarhzout*, Ali Ouadfel, Fouad Zinoun**

*LabMIA-SI, Department of Mathematics, Faculty of Science, Mohammed V University in Rabat, Morocco*

**Corresponding author:* bouchra.tarhzout@um5r.ac.ma

**Abstract.** As an interdisciplinary subject from graph theory, dynamical systems and biometry, we introduce the concept of structural graph of fingerprints. More precisely, we consider the normal forms associated to some categories of fingerprints and construct their structural graph on the Poincaré sphere, where the nodes are defined as being the components of the chain recurrent set corresponding to the underlying dynamical system. Then, we investigate whether these graphs qualify as DNA, in a sense to be specified. As will be seen, this approach has nothing to do with the structural methods used so far in fingerprints classification. It should be stressed, however, that if this approach can be of some use for a primary classification, the present work is born from a pure mathematical curiosity rather than from any biometric or forensic intention.

## 1. Introduction

The idea of using phase portraits of continuous dynamical systems in texture modelling goes back probably to the 80's of the last century, when an interdisciplinary program has been initiated by the Semiconductor Research Corporation at the University of Michigan to develop a visual language for representing visual data in semiconductor wafer processing. The thesis by Rao [14], for instance, was part of this program. Special mention must also be made of the thesis by Ford [4], at the University of Arizona, on 2-D fluid flow modelling and visualization, whereby complex flows were split into simpler and easily described components, the latter being modelized by linear phase portraits and then combined to obtain a global model for the entire flow field. This idea has been literally applied to fingerprints and recapitulated as a chapter by Li and Yau [8] where, following Kass and Witkin's [6] scheme of squaring the gradient vectors in the computed oriented texture field, basic fingerprint fixed points have been assimilated to either a Focus or a Saddle. More recently, the study conducted (and is still ongoing) by Zinoun [17] has introduced new ideas in the subject, pointing out that some fingerprint patterns cannot be modelized by

Received: Mar. 10, 2026.

2020 *Mathematics Subject Classification.* 37N25, 34C60, 37B20, 37G05.

*Key words and phrases.* fingerprint; normal form; dynamics at infinity; Poincaré sphere; structural graph; DNA.

https://doi.org/10.28924/2291-8639-24-2026-201
ISSN: 2291-8639

elementary fixed points with classical connections, thus inviting reflection on degenerate points and subtle connections from Saddle-Node, Takens-Bogdanov, Andronov-Hopf or Homoclinic-Loop bifurcations. So, Cusps have been proposed as good candidates for (a partial) modelling (of) the Deltas, and some fingerprint singularities and nearby orientational behavior will even be identified with a family of solution curves portrayed on a Poincaré section from a special case of the restricted planar three-body-problem, a fact which seems to have never been observed before. Then, the geometrical problem of the global representation of a fingerprint's flow-like stream of ridges as a smooth deformation of the phase portrait of a differential system has been formulated within Poincaré's index theory and addressed via a normal form approach as a bivariate Hermite interpolation problem. As a result, some preliminary models of the Circular/Elliptical Whorl, the Spiral, the Arch, the Loop, the Spiral in Loop, the Circlet in Loop and the Twist, have been obtained, and the normal forms of the Elliptical/Circular Whorl, the Spiral, the Arch and the Twist have been explicitly written down as second-order ordinary differential equations.

The present work deals with these normal forms. The structural graph (used in the sense of Osipenko [12], see also references therein) of a fingerprint will be derived from the global phase portrait on the Poincaré sphere of the associated normal form, "infinite" points on the equator being determined and topologically classified. The justification of a global phase portrait on the sphere, emphasing the points at infinity, lies in the fact that a fingerprint image is actually a projection on the plane of the "hemispherical" friction ridge surface of the finger, obtained by a nail-to-nail fingerprint rolling on an inking plate or an optical scanner. Then, it is shown, for example, that the structural graph of the Spiral and the Twist stands for a DNA of such fingerprints, in the sense that information encoded in the graph can be used to recover the entire phase portrait of the underlying system up to an orientation-preserving homeomorphism, which will be not the case for the Elliptical/Circular Whorl. Curiously, a huge literature has been devoted to the use of (oriented) graphs in pattern recognition, and a variety of graph-based fingerprint representations taking into account both minutiae features and the global ridge topology has been proposed (see for instance Marcialis et al. [10] for a brief survey and a comparison of these methods to the statistical approaches for fingerprint classification), but to the best of our knowledge, no interest was paid to their structural graph, in a dynamical sense. As will be seen, the notion of structural graph of (the normal form of) a fingerprint herein introduced has nothing to do with the structural approaches known so far for fingerprint classification, but could be considered as a first support to derive more occurate graphs to capture the ridges structure of fingerprints. For an updated edition which covers major topics in practical fingerprint recognition, feature extraction and matching methods, we refer to the handbook by Maltoni et al. [9].

The paper is organized as follows. Section 2 reviews several preliminary results that will serve as the foundation for the subsequent graphic analysis of fingerprint structures. Section 3 is devoted to the application of these results to fingerprint graphic modeling, where we show that the method also allows us to identify cases in which the resulting structure exhibits a DNA-like configuration.

In such cases, individuals within the same fingerprint category can be digitally — yet very roughly — identified for primary classification through their structural graph. And the last section is dedicated to some potential research perspectives.

## 2. Preliminaries

This section provides the theoretical background supporting our main contribution: encoding the fundamental topological structure of a dynamical system into its representative graph. We begin by recalling the concept of a structural graph. We then present the Poincaré sphere compactification as presented in Perko [13], which will later be used to locate and classify the fixed points at infinity.

### 2.1. **Chain Recurrent Set and Structural Graph.**

To lay the foundation for the structural graph, we begin by introducing a hierarchy of recurrence by formally defining its core elements, starting from fixed and periodic points and extending to recurrent, nonwandering and chain recurrent points.

#### 2.1.1. *Theoretical Framework for the Structural Graph.*

**Definition 2.1.** *A dynamical system on $E$ is a $C^1$-map*

$$\varphi : \mathbb{R} \times E \longrightarrow E$$

*where $E$ is an open subset of $\mathbb{R}^n$ and if $\varphi_t(x) = \varphi(t,x)$, then $\varphi_t$ satisfies*

i) $\varphi_0(x) = x$ *for all* $x \in E$ *and*
ii) $\varphi_t \circ \varphi_s(x) = \varphi_{t+s}(x)$ *for all* $s, t \in \mathbb{R}$ *and* $x \in E$.

It follows that for each $t \in \mathbb{R}$, $\varphi_t$ is a $C^1$-map of $E$ into $E$ which has a $C^1$-inverse, $\varphi_{-t}$. In other terms, $(\varphi_t)_{t\in\mathbb{R}}$ is a one-parameter family of diffeomorphisms on $E$ that forms a commutative group under composition. Besides, the function

$$f(x) = \frac{d}{dt}\varphi(t,x)|_{t=0}$$

defines a $C^1$-vector field on $E$ and for each $x_0 \in E$, $\varphi(t, x_0)$ is the solution of the initial value problem

$$\begin{cases} \dot{x} = f(x) \\ x(0) = x_0 \end{cases}$$

with the maximal interval of existence $I(x_0) = ]-\infty, +\infty[$.

**Definition 2.2.** 1. *The orbit (or trajectory) of $x \in E$ is the set $orb(x) := \{\varphi_t(x),\, t \in \mathbb{R}\}$. The natural order on the real line induces an orientation (or sense of motion) on $orb(x)$. The set $\{orb(x), x \in E\}$ of all (oriented) trajectories is called the phase portrait of $\varphi$, and the (possibly empty) sets*

$$\alpha(x) := \bigcap_{t\leq 0} \overline{\{\varphi_s(x), s \leq t\}}$$

$\omega(x) := \bigcap_{t\geq 0} \overline{\{\varphi_s(x), s \geq t\}}$,

*where $\bar{\cdot}$ means closure are, respectively, the $\alpha$-limit and the $\omega$-limit sets of $x$, or of $orb(x)$.*

2. *$x$ is called a fixed point if $\varphi_t(x) = x$ for all $t \in \mathbb{R}$, i.e. $orb(x) = \{x\}$. It is also called a critical, a singular, or an equilibrium point.*
3. *A non-fixed point $x$ is called periodic if there exists a $t \neq 0$ such that $\varphi_t(x) = x$. In such a case, $orb(x)$ is a closed orbit.*
4. *$x$ is a recurrent point if for any neighborhood $U$ of $x$ and $t > 0$, there exists $s > t$ such that $\varphi_s(x) \in U$.*
5. *$x$ is a nonwandering point if for each neighborhood $U$ of $x$ and $t > 0$, there is $s > t$ so that $\varphi_s(U) \cap U \neq \emptyset$.*
6. *Let $d$ be a metric on $E$. Given $\varepsilon > 0$, $T > 0$ and $x, y \in E$, an $(\varepsilon, T)$-chain from $x$ to $y$ is a pair of finite sequences $x = x_0, x_1, ..., x_{n-1}, x_n = y$ in $E$ and $t_0, ..., t_{n-1}$ in $[T, +\infty[$ such that $d(\varphi_{t_i}(x_i), x_{i+1}) < \varepsilon$ for $0 \leq i \leq n-1$.*
7. *Two points $x$ and $y$ are chain equivalent if for every $\varepsilon > 0$ and every $T > 0$ there exists an $(\varepsilon, T)$-chain from $x$ to $y$ and there exists an $(\varepsilon, T)$-chain from $y$ to $x$.*
8. *A point $x$ is called chain recurrent if $x$ is chain equivalent to itself.*

The following inclusions hold, where Per, $\Omega_0$, $\Omega$ and $Q$ are the sets of periodic, recurrent, nonwandering and chain recurrent points, respectively:

$$\text{Per} \subset \Omega_0 \subset \Omega \subset Q$$

2.1.2. *The Structural Graph.*

**Definition 2.3.** *A subset $q \subset Q$ refers to a component of the chain recurrent set if any two points from $q$ are chain equivalent.*

*The chain recurrent set can thus be decomposed into a union of disjoint, closed, invariant components $Q_i$:*

$$Q = \bigcup_{i\in I} Q_i,$$

*the set $I$ being not necessarily finite or countable.*

**Definition 2.4.** *Let $(Q_i)_{i\in I}$ be the family of components of the chain recurrent set. We say there is a connection $Q_i \to Q_j$ if there exists a point $x$ such that its $\alpha$-limit set satisfies $\alpha(x) \subset Q_i$ and its $\omega$-limit set satisfies $\omega(x) \subset Q_j$. In other words, there exists an orbit which "starts" in $Q_i$ and "ends" in $Q_j$.*

**Definition 2.5.** *The graph whose vertices $i$ correspond to the components $Q_i$ and whose edges $i \to j$ correspond to the connections $Q_i \to Q_j$ is called the* structural graph *of the dynamical system $\varphi$ and will be denoted $SG(\varphi)$.*

Interestingly, within the existing literature on structural graphs, fundamental topological properties such as connectedness, completeness and planarity have not been systematically investigated. This omission naturally raises an important question: how do the intrinsic properties of a

structural graph reflect the underlying dynamical properties of the associated dynamical system? In other words, what is the precise correspondence between graph-theoretical characteristics and dynamical behavior?

Before proceeding to the next section, we introduce a central notion that will guide the remainder of this work. Whenever a structural graph allows the reconstruction of the phase portrait of a dynamical system, up to an orientation-preserving homeomorphism, we designate this graph as the DNA of the system. Accordingly, we write $SG(DS) \equiv DNA(DS)$, emphasizing that the structural graph encodes the essential qualitative dynamics of the system. This concept will later serve as the foundation for our application to fingerprint structures. Here is a simple illustrative example showing how to extract (and to show the DNA character of) the structural graph of the classical van der Pol (*vdP*) system given by

$$\ddot{x} - \mu(1 - x^2)\dot{x} + x = 0,$$

where $\mu$ is a scalar parameter measuring the nonlinearity and the strength of the damping. The adaptive subdivision process (see, for instance, [12], p. 62) allows the localization of the chain recurrent set of a given system. For the van der Pol oscillator, the chain recurrent set consists of two distinct components: a fixed point $P$ and an isolated periodic orbit (limit cycle) $LC$, linked as follows

$$SG(vdP) = (\infty \to LC \leftarrow P)$$

Here, the symbol $\infty$ denotes the point at infinity added to $\mathbb{R}^2$ in order to obtain the compactified plane $\overline{\mathbb{R}^2}$, which is homeomorphic to the sphere $S^2$ (see section below).

We now explain how the phase portrait can be recovered—up to an orientation-preserving homeomorphism—from this structural graph. We first draw the periodic orbit $LC$, homeomorphic to a circle, and then determine the position of the fixed point relative to it. By Poincaré Index Theory, any periodic orbit in the plane contains at least one fixed point in its interior; if this fixed point is unique, it must be either a center or a focus. By construction, a node in a structural graph cannot correspond to a center or a center-focus in the finite case (much less a fixed point with an elliptic sector), and therefore the fixed point must be a focus $F$. The link $F \to LC$ indicates that the focus is repulsive, independently of the direction of spiraling. Although the structural graph does not explicitly state the stability of the limit cycle, the link $\infty \to LC$ implies the existence of at least one unbounded trajectory whose $\omega$-limit set is $LC$. Such a configuration can only occur if trajectories spiral toward the limit cycle, meaning that there exists an exterior neighborhood of $LC$ in which all trajectories behave similarly and intersect any transversal infinitely many times. Classical arguments based on the Jordan curve theorem (see Coddington and Levinson [3], p. 396) justify this behavior. By symmetry of reasoning applied to the interior via the link $F \to LC$, one concludes that the limit cycle is globally stable, in the sense that it attracts all orbits except the equilibrium point. The resulting qualitative "photofit" picture of the dynamics is therefore completely determined by the structural graph.

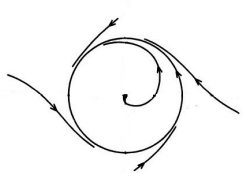

FIGURE 1. 'Photofit picture' of the dynamics of the van der Pol system.

The actual phase portrait of the van der Pol system is a continuous deformation of this photofit, possibly after reversing the orientation along the limit cycle and adjusting the spiraling direction of the focus by an appropriate choice of coordinate orientation. Consequently, the structural graph contains all the qualitative information about the dynamics, and we may write

$$SG(vdP) \equiv DNA(vdP)$$

In other words, the entire dynamical behavior of the van der Pol system in the phase plane can be encoded symbolically as $\infty \to LC \leftarrow F$. While this encoding appears natural in this classical example, isolating the DNA of a general dynamical system, that is the "simplest" graph (if it is not the structural graph itself) allowing the reconstruction of the phase portrait up to an orientation-preserving homeomorphism, is in general a far more delicate problem.

2.2. **Poincaré Sphere and Behavior at Infinity.** A classical method for studying trajectories at infinity is the Poincaré sphere compactification, which maps points at infinity onto its equator. As extensively treated in Lefschetz [7] and Perko [13], this technique provides a fully global description of the phase portrait, incorporating both finite and infinite dynamics.

The Poincaré sphere is defined to be the unit sphere

$$S^2 = \{(X, Y, Z) \in \mathbb{R}^3 / X^2 + Y^2 + Z^2 = 1\},$$

such that its north (or south) pole is tangent to the $(x, y)$-plane at the origin. Points on the $(x, y)$-plane can be mapped on the surface of the upper hemisphere by projecting lines passing by the centre of the sphere. This mapping is provided by the change of variables

$$X = xZ, \qquad Y = yZ, \qquad Z = \frac{1}{\sqrt{1 + x^2 + y^2}}$$

these equations define a one-to-one correspondence between points $(X, Y, Z)$ on the upper hemisphere of $S^2$ with $Z > 0$ and points $(x, y)$ in the plane. The origin $0 \in \mathbb{R}^2$ corresponds to the north pole $(0, 0, 1) \in S^2$, points on the circle $x^2 + y^2 = 1$ correspond to points on the circle $X^2 + Y^2 = 1/2$, $Z = 1/\sqrt{2}$ on $S^2$; and points on the equator of $S^2$ correspond to the “circle at infinity” or “points at infinity” of $\mathbb{R}^2$. The flow near antipodal points is topologically equivalent, though its direction may be reversed.

The following two theorems can be used to determine the flow at infinity. Only the statements of the theorem will be provided, but the reader interested in the details can find them in Perko [13]. From now on, the dynamical systems we deal with are defined by the flow associated to a planar differential system of the form

$$\begin{cases} \dot{x} = P(x,y) \\ \dot{y} = Q(x,y) \end{cases} \tag{*}$$

where $P$ and $Q$ are polynomial functions in $x$ and $y$. Let $m$ denote the maximum polynomial degree of the terms in $P$ and $Q$ and let $P_m$ and $Q_m$ be the higher terms of the corresponding polynomial functions $P$ and $Q$.

**Theorem 2.1.** *The critical points at infinity of the system (*) lie on the points $(X, Y, 0)$ of the equator of the Poincaré sphere where $X^2 + Y^2 = 1$ and*

$$XQ_m(X,Y) - YP_m(X,Y) = 0, \tag{2.1}$$

*or equivalently, at the polar angles $\theta_j$ and $\theta_j + \pi$ satisfying*

$$G_{m+1}(\theta) := \cos\theta\, Q_m(\cos\theta, \sin\theta) - \sin\theta\, P_m(\cos\theta, \sin\theta) = 0,$$

*which, if not identically zero, has at most $m+1$ pairs $\theta_j$ and $\theta_j + \pi$. Moreover, if $G_{m+1}(\theta)$ is not identically zero, the flow on the equator of the Poincaré sphere is clockwise (counter-clockwise) at points corresponding to polar angles $\theta$ where $G_{m+1}(\theta) < 0$ ($G_{m+1}(\theta) > 0$).*

Note that the points at infinity of $\mathbb{R}^2$ will always come in pairs since the projective lines intersect the equator of the Poincaré sphere twice as $\|x\| \to +\infty$.

The behavior of the flow in a neighborhood of any critical point on the equator of $S^2$, i.e. the topological nature of the critical points at infinity, can then be described projecting the flow on the Poincaré sphere onto the two planes $(x, z)$ and $(y, z)$ tangent to the equator points $Y = 1$ and $X = 1$ respectively. This is summarised in the following.

**Theorem 2.2.** *The flow on the Poincaré sphere in the neighborhood of any critical point on the equator, except the points $(0, \pm 1, 0)$, is topologically equivalent to the flow defined by the system*

$$\begin{cases} \pm\dot{y} = yz^m P\left(\frac{1}{z}, \frac{y}{z}\right) - z^m Q\left(\frac{1}{z}, \frac{y}{z}\right) \\ \pm\dot{z} = z^{m+1} P\left(\frac{1}{z}, \frac{y}{z}\right) \end{cases} \tag{1}$$

*where the direction of the flow is determined from $G_{m+1}(\theta)$.*

*Similarly, the flow on the Poincaré sphere in the neighborhood of any critical point on the equator, except the points $(\pm 1, 0, 0)$, is topologically equivalent to the flow defined by the system*

$$\begin{cases} \pm\dot{x} = xz^m Q\left(\frac{x}{z}, \frac{1}{z}\right) - z^m P\left(\frac{x}{z}, \frac{1}{z}\right) \\ \pm\dot{z} = z^{m+1} Q\left(\frac{x}{z}, \frac{1}{z}\right) \end{cases} \tag{1'}$$

*where the direction of the flow is determined from $G_{m+1}(\theta)$.*

Moreover, if $m$ is odd, the antipodal points on $S^2$ are qualitatively equivalent and if $m$ is even, the antipodal points are qualitatively equivalent but the direction of the flow is reversed.

Furthermore, there is a direct correspondence between equilibria of the auxiliary systems and the actual equilibria on the equator:

- a fixed point of (1) at $(y_0, 0)$ corresponds to

$$\left( \frac{1}{\sqrt{1+y_0^2}}, \frac{y_0}{\sqrt{1+y_0^2}}, 0 \right),$$

- a fixed point of (1′) at $(x_0, 0)$ corresponds to

$$\left( \frac{x_0}{\sqrt{1+x_0^2}}, \frac{1}{\sqrt{1+x_0^2}}, 0 \right).$$

Once the dynamics at infinity are incorporated through the Poincaré sphere, one can naturally check compatibility with (a direct consequence of) the well-known Poincaré Index Theorem:

$$I_\varphi(S^2) = 2,$$

$I_\varphi(S^2)$ being the sum of the indices of the fixed points of $\varphi$, in particular, for a number $n$ of Nodes, $f$ of Foci and $s$ of Saddles:

$$n + f - s = 2$$

## 3. Structural Graph of Fingerprints

Having established the necessary groundwork, we now apply these results to fingerprint graphic modelling. Specifically, we construct the structural graphs associated with the principal fingerprint categories and examine the cases in which the resulting configurations exhibit a DNA-like organization. This perspective, as previously stated, offers a preliminary method—born from a purely mathematical curiosity rather than from any biometric intention—to encode and classify individuals sharing the same fingerprint pattern through their structural graph. This builds directly upon the work of Zinoun [17], from which several illustrative figures have been adapted. It should be noted, however, that Zinoun's construction of structure-preserving normal forms could be achieved only for a restricted number of configurations within the well-known Purkyně–Galton classification [5]. While the Elliptical/Circular Whorl, the Spiral, and the Twist, admit explicit analytical representations through low-degree polynomial systems, other patterns such as Loops and Double Whorls resist such reduction. This limitation stems from the index-theoretic constraints governing the coexistence of fixed points and from the non-poised nature of the underlying Hermite interpolation problem, particularly when singularities occur at infinity. Consequently, Zinoun

limits his analysis to configurations involving a small number of singularities—typically one Center or Focus and two Cusps—each serving as a canonical prototype from which other fingerprint types may be conceptually derived (see [17] for details).

Following Poincaré's methodology, as presented in Perko [13], equation $(2.1)$ is solved to locate the fixed points at infinity on the equator of the Poincaré sphere, while the auxiliary systems (1) or (1') (depending on the position on the equator) are qualitatively studied to determine the topological nature of these points. Once this step is completed, the global phase portrait of the system can be intuitively reconstructed. The flow is drawn as if you are looking straight at the $xy$-plane: the $x$-axis is taken as the horizontal direction, the $y$-axis is the vertical direction and the $z$-axis points toward the observer (out of the plane).

The northern hemisphere $(z > 0)$ corresponds to finite points $(x, y)$ of the plane. The equator $(z = 0)$ represents the points at infinity. The southern hemisphere $(z < 0)$ mirrors the behavior of the northern one under antipodal symmetry. Hence, the equilibrium at infinity first appears on the equator. At each equatorial point $(x, y, 0)$, its antipodal point $(-x, -y, 0)$ represents the opposite direction at infinity. Coherence is then verified through the Poincaré Index Theorem, ensuring that the sum of the indices of all fixed points on the sphere is equal to 2. This guarantees that the resulting spherical portraits are both topologically consistent and dynamically meaningful.

Finally, the structural graph is extracted, providing a concise symbolic encoding of the global dynamics. This graph serves as the foundation for distinguishing and classifying the principal fingerprint categories within the proposed dynamical framework.

3.1. **The Elliptical/Circular Whorl.** In [17], after identifying the mathematical limitations of previous methods— mainly those relying on linearization around fixed points of the first species— the author introduces a structure-preserving normal form approach capable of connecting multiple fixed points within a global (yet idealized) configuration. Focusing first on the Elliptical/Circular Whorl (Figure 2), he considers a configuration composed of a Center at the origin of the $(x, y)$ plane, representing the fingerprint's core, and two Cusps placed symmetrically at $\pm(1, 0)$, representing the Deltas. He then formulates the problem as a bivariate Hermite interpolation task, seeking a smooth symmetric vector field whose trajectories connect these singularities while preserving their qualitative nature. Solving this problem leads to the normal (or idealized) form

$$\begin{cases} \dot{x} = y \\ \dot{y} = -x\,(x^2 - 1)^2 \end{cases} \tag{2}$$

whose phase portrait (see Figure 3) reproduces the structural organization of fingerprints of Elliptical/Circular Whorl type.

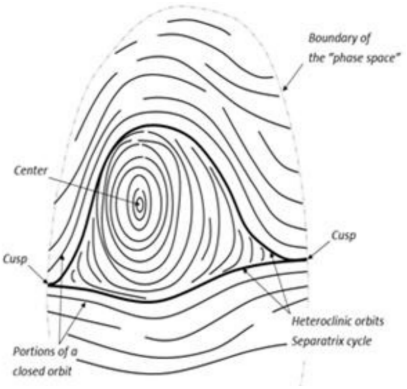


FIGURE 2. Preliminary modelling of the Elliptical/Circular Whorl.

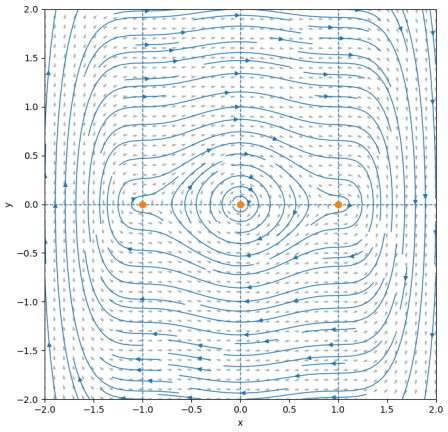


FIGURE 3. Computer-drawn phase portrait of system (2).

The Center at the origin of this system projects, under the central projection, onto Centers at the north and south poles of $S^2$. The fixed points at infinity for this system are determined by the solutions of

$$X^2 + Y^2 = 1 \quad \text{and} \quad XQ_5(X,Y) - YP_5(X,Y) = -X^6 = 0,$$

i.e., there are fixed points on the equator of $S^2$ at $\pm(0,1,0)$. Also, we see from this expression that the flow on the equator of $S^2$ is clockwise (for $X > 0$ (or $X < 0$) the above quantity is negative). The behavior at $(0,1,0)$ is determined by the behavior of the system

$$\begin{cases} \dot{x} = -z^4 - x^6 + 2x^4z^2 - x^2z^4 \\ \dot{z} = -x^5z + 2x^3z^3 - xz^5 \end{cases} \tag{3}$$

at the origin. The Jacobian matrix at origin $(0,0)$ is zero, revealing a fully degenerate equilibrium. The linear approximation provides no information about the local dynamics: Hartman-Grobman Theorem is obviously not applicable, so the characterization of the origin requires more elaborated

approaches. Observe that system (3) is already in Poincaré-Dulac normal form, that is

$$[S, f] = 0,$$

where $f$ is the vector field associated to system (3), $S$ the semi-simple part of its Jacobian matrix $A$ at the origin, and $[.,.]$ is the usual Lie bracket of vector fields. It is also in Belitskiĭ's normal form [2], i.e.:

$$[A^*, f] = 0,$$

$A^*$ being the conjugate transpose of $A$. So, this requires a further reduction to normal form, say a renormalization, which is sometimes possible in the presence of Lie-point symmetries, that is nonlinear vector fields $g$ satisfying

$$[f, g] = 0$$

In fact, in such case, and to renormalize system (3), we could fruitfully use the Poincaré Code, a Maple normal form package written by F. Zinoun in the 90's and published later as a theoretical paper in [11], and particularly the Poincaré_Dulac_JNF command which computes a joint normal form both for the vector field under study and its Lie-point symmetry (see example 12 in [11]). We know that the case of a quadratic leading part can be dealt with within a normal form approach (see for instance Strozyna [15]), but to our knowledge, no general program for higher-order leading part is available in the literature. Besides, no trivial symmetry can be derived from system (3), as it would be horrible to try to conduct by hand such computations to sufficiently higher orders. So, even though it does not stand for a mathematical proof, we simply proceed to a numerical simulation of system (3) to explore the structure of the trajectories near the equilibrium. It follows that the origin behaves as a Cusp-like singularity. The behavior at the antipodal point $(0, -1, 0)$ is exactly the same as the behavior at $(0, 1, 0)$, i.e., there is also Cusp-like singularity at $(0, -1, 0)$, since $m = 5$ is odd in this example.

The flow on the unit disk shown in Figure 4 is referred to as the global phase portrait for the system (2) since it describes the behavior of every trajectory of the system including the behavior of the trajectories at infinity. The global phase portrait of the system on the sphere reduces to a continuous family of closed orbits, degenerating into two Centers on the poles, and punctuated by an equatorial separatrix cycle and another one on each hemisphere, as illustrated below ($C$ for the polar Center, $C_{1,2}$ for the two hemispherical and heteroclinicly joint Cusps, and $C^{\infty}_{1,2}$ for the equatorial and antipodal Cusps):

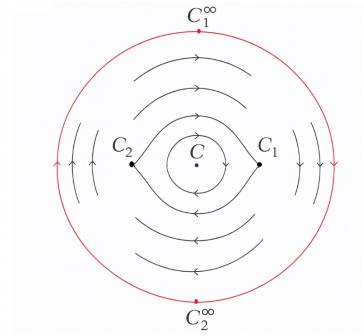


FIGURE 4. The global phase portrait for the system (2).

As pointed out before, compatibility with Poincaré Index Theory can be checked on the sphere: the index of a Center is obviously equal to 1, and for a Cusp, one can use Bendixon formula giving the index $I$ of a singular point in terms of the numbers $e$ and $h$ of its elliptic and hyperbolic sectors, respectively:

$$I = 1 + \frac{e-h}{2},$$

which leads to a zero index for a Cusp $(e = 0, h = 2)$.

The same formula shows that there is no singular point with three, and only three, hyperbolic sectors, hence the difficulty in the modelization of the Delta [17].

Finally, the corresponding structural graph degenerates into a trivial graph consisting of a single vertex representing the whole sphere $S^2$, and is therefore not of the DNA type. If this carries no topological significance for the corresponding fingerprint, as will be seen, it is not the case for the following class.

3.2. **The Spiral.** The same structure-preserving methodology is applied, but with a key modification affecting both the central and global dynamics. In this case, the Center of the Elliptical/Circular Whorl is replaced by a Focus, thereby introducing a rotational component into the flow and breaking the strict symmetry of the previous configuration. Moreover, the separatrix cycle that bounded the inner trajectories in the Elliptical/ Circular Whorl case disappears, giving rise to an unbounded spiral motion.

To reproduce this configuration, a system composed of a Focus at the origin—representing the fingerprint's core—and two Cusps symmetrically placed at $x = \pm 1$, corresponding to the Deltas, is considered. By formulating a bivariate Hermite interpolation problem with adjustable parameters controlling both damping and rotation, these local structures are unified into a single analytic system. Solving this problem leads to the normal form

$$\begin{cases} \dot{x} = y \\ \dot{y} = \left(y - \frac{x}{2}\right)(x^2 - 1)^2 \end{cases} \tag{4}$$

whose phase portrait resembles the damped pendulum's (see Figure 6), but with Cusps instead of Saddles. The two external Cusps are preserved, while the central singularity becomes a Focus, generating the open spiral trajectories that characterize this fingerprint subclass within the broader Whorl family.

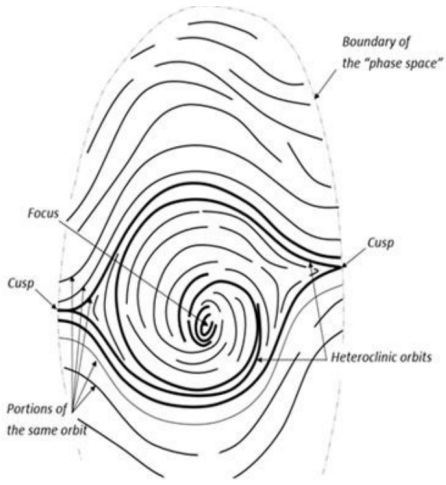


FIGURE 5. Preliminary modelling of the Spiral.

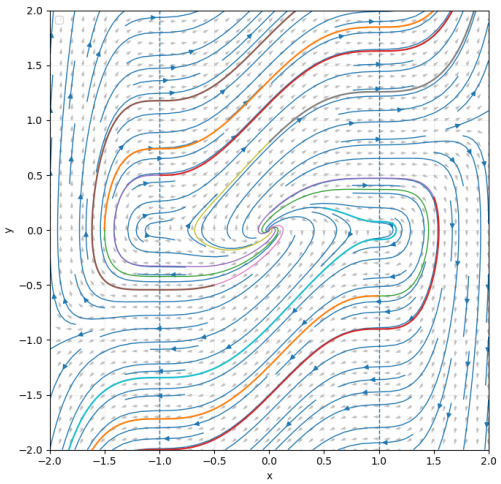


FIGURE 6. Computer-drawn phase portrait of system (4).

The Focus at the origin of this system projects, under the central projection, onto Foci at the north and south poles of $S^2$. The fixed points at infinity for this system are determined by the solutions of

$$XQ_5(X,Y) - YP_5(X,Y) = X^5(Y - \frac{X}{2}) = 0,$$

together with $X^2 + Y^2 = 1$. That is, the fixed points at infinity are at $\pm(0,1,0)$ and $\pm(2,1,0)/\sqrt{5}$. The behavior near each of the fixed points $(0,1,0)$ and $(2,1,0)/\sqrt{5}$ on $S^2$ is determined by the

behavior of the system

$$\begin{cases} -\dot{x} = -z^4 + x^5 - 2x^3z^2 + xz^4 - \dfrac{x^6}{2} + x^4z^2 - \dfrac{x^2z^4}{2} \\ -\dot{z} = z^5 + x^4z - 2x^2z^3 - \dfrac{x^5z}{2} + x^3z^3 - \dfrac{xz^5}{2} \end{cases} \tag{5}$$

near the fixed points $(0,0)$ and $(2,0)$, respectively. For this system, with $f$ as the vector field, we have

$$Df(0,0) = 0 \quad \text{and} \quad Df(2,0) = \begin{bmatrix} -16 & 0 \\ 0 & 0 \end{bmatrix}$$

As for system (3), the behavior near the origin is confirmed by numerical simulation, which shows that the origin $(0,0)$ is a stable Node. To unveil the topological nature of the point $(2,0)$, we have particularly used the Poincaré_Dulac_Walcher command of the Poincaré Code package, which implements Walcher's algorithm for computation of (structure-preserving) normal forms near a singular point [16].

The first terms of the 5th-order normal form are

$$\begin{cases} \dot{x} = -16x \\ \dot{z} = \dfrac{z^5}{2} \end{cases}$$

and it follows that the singular point is topologically a Saddle. Note that computation of the normal form is necessary to obtain this information. Since $m$ is odd, the behavior near the antipodal points $(0,-1,0)$ and $(-2,-1,0)/\sqrt{5}$ is qualitatively equivalent to the behavior at $(0,1,0)$ and $(2,1,0)/\sqrt{5}$ respectively. In Figure 7 the global phase portrait for the dynamical system (4) has been drawn.

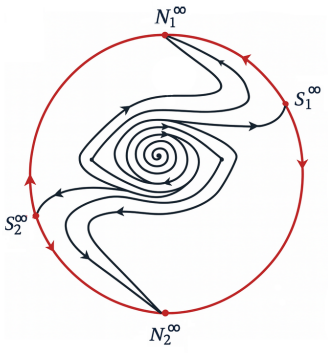


FIGURE 7. The global phase portrait for the system (4).

With obvious notation, the corresponding structural graph can be then represented schematically as

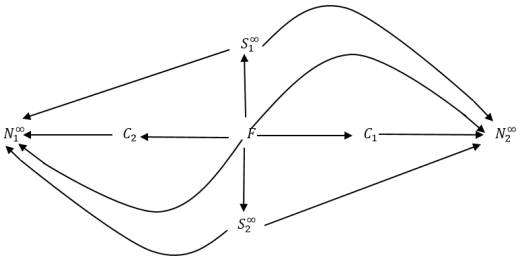


Recall that the structural graph is a topological invariant, i.e. two topologically equivalent differential systems will share the same graph. In this regard, the graph above stands for the structural graph of the Spiral, as shown in Figure 5, not only for its normal (or idealized) form.

**Proposition 3.1.** *With obvious notation,*

$$SG(4) \equiv DNA(4)$$

*Proof.* To prove that the phase portrait of $(4)$ on the Poincaré sphere can be uniquely reconstructed (up to an orientation-preserving homeomorphism) from the information encoded in the graph, note that, when the points at infinity appear as nodes of the structural graph, their relative disposition with respect to each other on the equator is immediately known. Note also that, unlike the van der Pol system, the Focus has to be designated as such in the graph because it is not confined in what could be a Cusp-Cusp separatrix cycle. So let's start with that point. The links "$F \to C_1 \to N_2^\infty$" (and similarly for "$F \to C_2 \to N_1^\infty$") inform both about the stability of the Focus and about an heteroclinic orbit joining a Cusp, which stands for the stable manifold of that point, while its unstable manifold is supported by another heteroclinic orbit joining a Node. This configuration can be realized in two "symmetric" manners, as illustrated below:

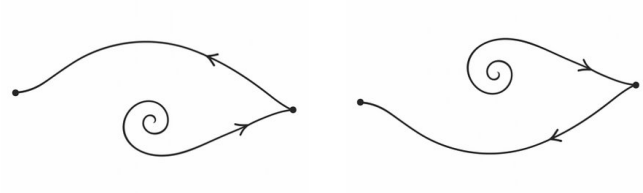

Note that, however, if the sense of motion on the orbits (the orientation of the graph) has no effect on the description of the fingerprint ridges, the configuration above does matter in fingerprints comparison.

Besides, if we place the Focus, the two Cusps and the two infinite Nodes on the same semi-circular line on the hemisphere, which is topologically legitimate, the antipodal character of the Nodes may suggest that the Cusps are naturally situated on both sides of the Focus, but this is not

the only possible configuration. In other terms, the following eye-like motif is guaranteed only up to a continuous deformation of the phase portrait:

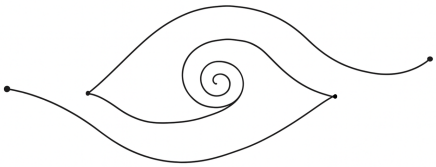

Let now consider the links $S_1^\infty \leftarrow F \rightarrow S_2^\infty$ and $N_1^\infty \leftarrow S_i^\infty \rightarrow N_2^\infty$, for $i = 1, 2$. It follows that, obviously, for each Saddle $S_i^\infty$, there is a separatrix trajectory $\Gamma_i^1$ such that, with some abusive notation, $\alpha(\Gamma_i^1) = F$, and two other separatrices $\Gamma_i^j$, $j = 2, 3$, satisfying $\omega(\Gamma_i^j) = N_i^\infty$.

We know that the infinite Saddles and Nodes are alternatively distributed on the equator, where two neighboring points are sharing a common sector, hyperbolic for the Saddle, parabolic for the Node. Moreover, they are joined by equatorial (heteroclinic) orbits. This obvious fact can be rigorously checked by using the following result, proved in Andronov [1]: If the polynomials $P$ and $Q$ in (*) begin with mth-degree terms $P_m(x, y)$ and $Q_m(x, y)$ with $m \geq 1$, and if $xQ_m(x, y) - yP_m(x, y)$ is not identically zero, then any definite direction of approach $\theta_0$ of the origin satisfies the equation

$$\cos\theta_0\, Q_m(\cos\theta_0, \sin\theta_0) - \sin\theta_0\, P_m(\cos\theta_0, \sin\theta_0) = 0$$

For system (5), this equation simply reads $\sin\theta_0 = 0$, which confirms the equatorial character of the heteroclinic Saddle-Node orbits. Finally, gathering all these informations leads to the global phase portrait drawn in Figure 7, up to an orientation-preserving homeomorphism, and possibly, a permutation of the hemispheres. □

3.3. **The Twist.** The Twist, like the Spiral, arises as a subclass of the Whorl configuration. It is obtained by replacing the Elliptical/Circular Whorl's central Center (or the Focus of the Spiral) by an Improper Node, while keeping two Cusps at the periphery. Following the same procedure used for previous categories, a system whose local phase portraits correspond to these singularities is constructed. The Improper Node replaces the central Focus or Center, thereby introducing an asymmetric convergence of trajectories toward the core. The two Cusps are again positioned symmetrically at $x = \pm 1$, representing the Deltas. By enforcing smooth connections between these three local structures while preserving their qualitative nature, the problem once more reduces to a Hermite interpolation setting. Solving this interpolation under the same constraints as before leads to the normal form

$$\begin{cases} \dot{x} = y, \\ \dot{y} = (2y - x)(x^2 - 1)^2 \end{cases} \tag{6}$$

This polynomial vector field generates a phase portrait (see Figure 9) in which the central Improper Node distributes trajectories toward the two Cusps in a twisted manner, thereby capturing the essential topological and geometric features of the Twist fingerprint.

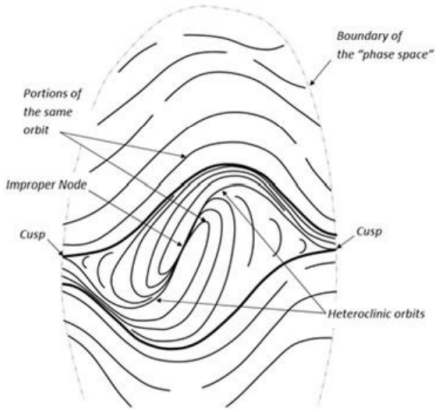


FIGURE 8. Preliminary modelling of the Twist.

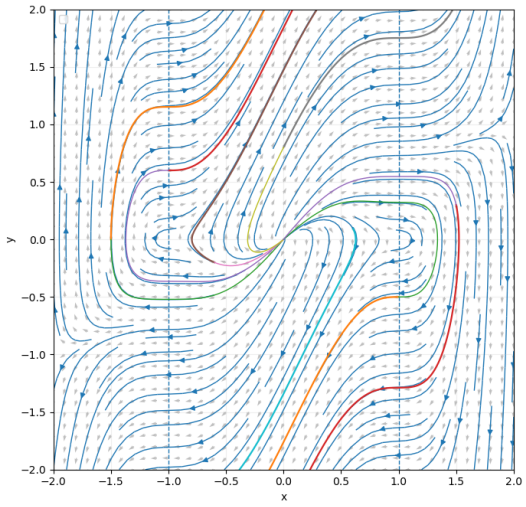


FIGURE 9. Computer-drawn phase portrait of system (6).

The Node at the origin of this system projects, under the central projection, onto Nodes at the north and south poles of $S^2$. The fixed points at infinity for this system are determined by the solutions of

$$XQ_5(X,Y) - YP_5(X,Y) = X^5(2Y - X) = 0,$$

together with $X^2 + Y^2 = 1$. That is, there are fixed points on the equator of $S^2$ at $\pm(0,1,0)$ and $\pm(2,1,0)/\sqrt{5}$. The behavior near each of the fixed points $(0,1,0)$ and $(2,1,0)/\sqrt{5}$ is determined

by the behavior of the system

$$\begin{cases} -\dot{x} = -z^4 + 2x^5 - 4x^3z^2 + 2xz^4 - x^6 + 2x^4z^2 - x^2z^4 \\ -\dot{z} = 2z^5 + 2x^4z - 4x^2z^3 - x^5z + 2x^3z^3 - xz^5 \end{cases} \tag{7}$$

near the fixed points $(0,0)$ and $(2,0)$, respectively. For this system, with $f$ as the vector field, we have

$$Df(0,0) = 0 \quad \text{and} \quad Df(2,0) = \begin{bmatrix} -32 & 0 \\ 0 & 0 \end{bmatrix}$$

As for systems (3) and (5), the nature of the origin will be determined by a numerical integration of the nonlinear system (7) that shows that the origin $(0,0)$ is a stable Node. At $(2,0)$, we again used the same Poincaré Code normal form Maple package to unveil the topological nature of the point. The first terms of the 5th-order normal form are

$$\begin{cases} \dot{x} = -32x \\ \dot{z} = \dfrac{z^5}{2} \end{cases}$$

from which it follows that the singular point is topologically a Saddle. The behavior near the antipodal points $(0,-1,0)$ and $(-2,-1,0)/\sqrt{5}$ is exactly the same as the behavior at $(0,1,0)$ and $(2,1,0)/\sqrt{5}$ respectively, since m is odd. It then follows that the global phase portrait for the system in this case is given as in Figure 10.

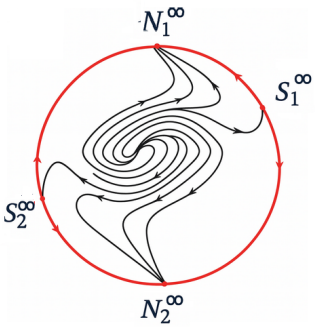


FIGURE 10. The global phase portrait for the system (6).

The corresponding structural graph can be then represented schematically as

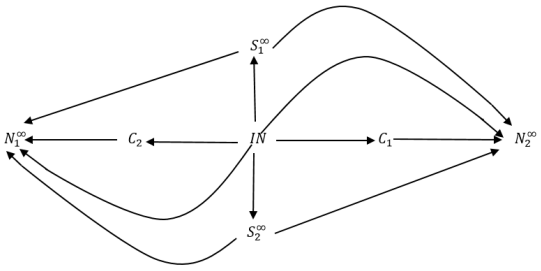


The Twist configuration is analogous to the Spiral; it also corresponds to a DNA, following the same reasoning as in the previous proof, with the only difference being that the Focus is replaced by an Improper Node. We know that these points are homeomorphic, but not diffeomorphic.

3.4. **The Tented Arch.** In [17], the Cusp does not constitute a complete fingerprint category on its own but rather serves as a fundamental local singularity—a canonical building block from which more elaborate configurations are constructed. Each Delta point appearing in the Whorl, Spiral, or Twist patterns corresponds locally to such a Cusp. The dynamics near this point are governed by a nilpotent planar system, whose qualitative behavior is determined by higher-order terms.

The simplest representative of this class is given by

$$\begin{cases} \dot{x} = y^2 \\ \dot{y} = -x \end{cases} \tag{8}$$

whose phase portrait represented in Figure 12 reproduces the structural organization of fingerprints of Tented Arch type.

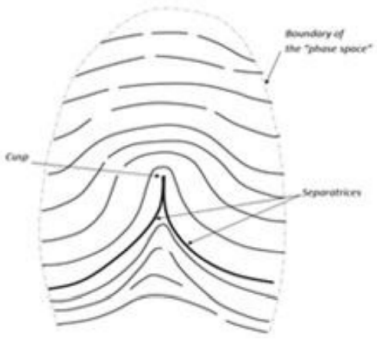


FIGURE 11. Preliminary modelling of the Tented Arch.

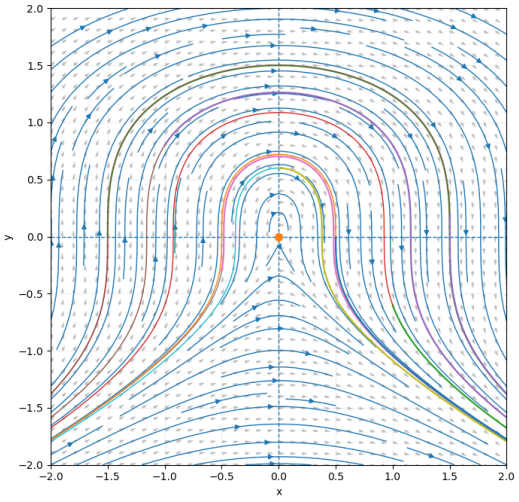


FIGURE 12. Computer-drawn phase portrait of system (8).

The fixed points at infinity for this system are determined by the solutions of

$$XQ_2(X,Y) - YP_2(X,Y) = -Y^3 = 0,$$

together with $X^2 + Y^2 = 1$. Thus, the only critical points at infinity are at $\pm(1,0,0)$. Also, we see from this expression that the flow on the equator of $S^2$ is clockwise for $Y > 0$ and counter-clockwise for $Y < 0$. The behavior at $(1,0,0)$ is determined by the behavior of the nilpotent system

$$\begin{cases} -\dot{y} = z + y^3 \\ -\dot{z} = y^2 z \end{cases} \tag{9}$$

at the origin.

As for systems (3), (5) and (7), the nature of the origin will be determined by numerical integration of system (9) that shows that the origin is a stable Node. The behavior at the antipodal point $(-1,0,0)$ is topologically equivalent to the behavior at $(1,0,0)$ with the direction of the flow reversed since $m$ is even in this example; i.e., $(-1,0,0)$ is an unstable Node. The global phase portrait of system (8) on the sphere $S^2$ is topologically equivalent to that of in Figure 13.

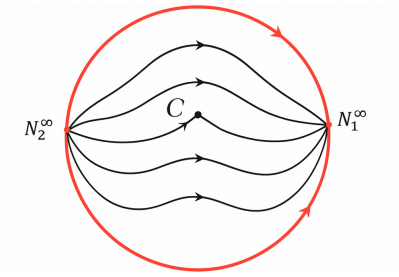


FIGURE 13. The global phase portrait of the system (8).

The corresponding structural graph can be then schematically represented as

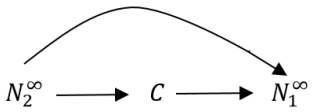


from which the DNA structure follows immediately.

## 4. Conclusion

In this work, we have applied the concept of structural graphs, originally developed for dynamical systems, to the study of fingerprint orientation fields. By interpreting fingerprints as smooth deformations of planar phase portraits, we have shown that their cores and deltas can be often characterized as dynamical singularities whose global configuration can be compactly represented on the Poincaré sphere. Through this compactification, both the finite and infinite behaviors of the system are brought together within a unified geometric setting, revealing the general dynamical structure of the fingerprint under study. The analysis of the corresponding normal forms and their projections onto the sphere has allowed us to identify the nature and interconnections of all equilibrium points, leading naturally to the extraction of their structural graphs. These graphs provide a primary digital representation of fingerprint patterns, and in specific configurations, they exhibit the features of a DNA-like structure—one that uniquely encodes the essential dynamics of the system.

As established earlier, the scope of this work was deliberately limited to four fingerprint categories—the Elliptical/Circular Whorl, the Spiral, the Twist, and the Tented Arch. This restriction was necessitated by the prerequisite of having well-defined normal forms for each category, which serve as the foundational templates for our structural graph approach. Future research will systematically extend this methodology to the remaining major fingerprint types: the Loop (Figure 14a), the Spiral in Loop (Figure 14b), and the Circlet in Loop (Figure 14c). The initial phase will focus on deriving their respective normal forms, a process that involves identifying the configuration that captures each pattern's essential topological structure. Subsequently, the corresponding structural graphs will be extracted from these normalized representations. This expansion is expected to provide a comprehensive framework for the classification and unique identification of all major fingerprint types, moving towards a complete topological taxonomy.

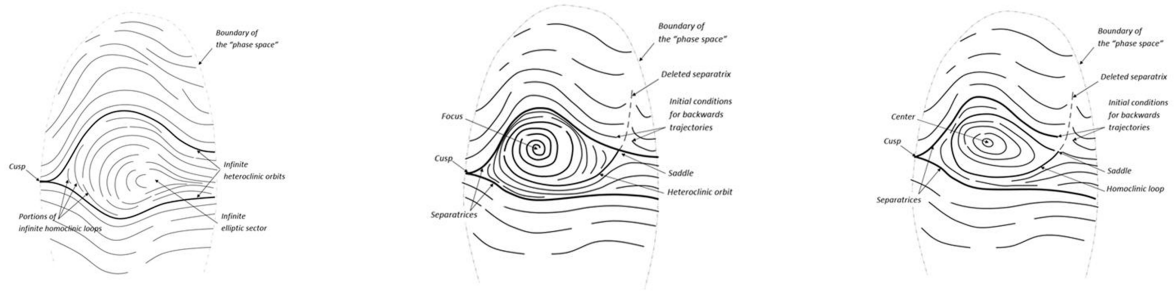


(A) (B) (C)

FIGURE 14. Preliminary modelling of the Loop (a), the Spiral in Loop (b) and the Circlet in Loop (c).

**Conflicts of Interest:** The authors declare that there are no conflicts of interest regarding the publication of this paper.

## REFERENCES

[1] A.A. Andronov, E.A. Leontovich, I.I. Gordon, A.G. Maier, Qualitative Theory of Second-Order Dynamical Systems, John Wiley & Sons, New York, 1973.
[2] G.R. Belitskiĭ, Normal Forms, Invariants and Local Mappings, Naukova Dumka, Kiev, 1979.
[3] E.A. Coddington, N. Levinson, Theory of Ordinary Differential Equations, McGraw-Hill, New York, 1955.
[4] R.M. Ford, Image Models for Flow Field Analysis, Representation, and Compression: A Dynamical System Approach, PhD thesis, University of Arizona, 1994.
[5] F. Galton, Finger Prints, Macmillan and Co., (1892).
[6] M. Kass, A. Witkin, Analyzing Oriented Patterns, Comput. Vis. Graph. Image Process. 37 (1987), 362–385. https://doi.org/10.1016/0734-189X(87)90043-0.
[7] S. Lefschetz, Differential Equations: Geometric Theory, Interscience, New York, 1957.
[8] J. Li, W.Y. Yau, Constrained Non-linear Phase Portrait Model of Fingerprint Orientation and Its Application to Fingerprint Classification, in: Advanced Topics in Biometrics, World Scientific, 2011: pp. 177–226. https://doi.org/10.1142/9789814287852_0008.
[9] D. Maltoni, D. Maio, A.K. Jain, J. Feng, Handbook of Fingerprint Recognition, Springer, 2022.
[10] G.L. Marcialis, F. Roli, A. Serrau, Graph-Based and Structural Methods for Fingerprint Classification, in: Applied Graph Theory in Computer Vision and Pattern Recognition, Springer, Berlin, 2007. https://doi.org/10.1007/978-3-540-68020-8_8.
[11] J. Mikram, F. Zinoun, A. El Abdllaoui, Poincaré Code: a Package of Open-Source Implements for Normalization and Computer Algebra Reduction near Equilibria of Coupled Ordinary Differential Equations, Comput. Phys. Commun. 184 (2013), 2204–2213. https://doi.org/10.1016/j.cpc.2013.04.003.
[12] G. Osipenko, Dynamical Systems, Graphs, and Algorithms, Springer, New York, 2006.
[13] L. Perko, Differential Equations and Dynamical Systems, Springer, New York, 2013.
[14] A.R. Rao, A Taxonomy for Texture Description and Identification, Springer, 1990.
[15] E. Stróżyna, Normal Forms for Germs of Vector Fields with Quadratic Leading Part. The Remaining Cases, Stud. Math. 239 (2017), 133–173. https://doi.org/10.4064/sm8627-2-2017.
[16] S. Walcher, On Transformations into Normal Form, J. Math. Anal. Appl. 180 (1993), 617–632. https://doi.org/10.1006/jmaa.1993.1420.

[17] F. Zinoun, Can a Fingerprint Be Modelled by a Differential Equation?, arXiv:1802.05671, 2018. https://doi.org/10.48550/arXiv.1802.05671.